MDPI

Article

The Effectiveness in Activating M-Type K$^+$ Current Produced by Solifenacin ([(3R)-1-azabicyclo[2.2.2]octan-3-yl](1S)-1-phenyl-3,4-dihydro-1H-isoquinoline-2-carboxylate): Independent of Its Antimuscarinic Action

Hsin-Yen Cho [1],[†], Tzu-Hsien Chuang [1],[†] and Sheng-Nan Wu [1,2],*

[1] Department of Physiology, National Cheng Kung University Medical College, Tainan City 70101, Taiwan;
    lilyzhou861126@gmail.com (H.-Y.C.); fytg55qq@gmail.com (T.-H.C.)
[2] Institute of Basic Medical Sciences, National Cheng Kung University Medical College,
    Tainan City 70101, Taiwan
[*] Correspondence: snwu@mail.ncku.edu.tw; Tel.: +886-6-2353535-5334; Fax: +886-6-2362780
[†] H.-Y.C. and T.-H.C. are equal contribution to the present work.

Abstract: Solifenacin (Vesicare$^®$, SOL), known to be a member of isoquinolines, is a muscarinic antagonist that has anticholinergic effect, and it has been beneficial in treating urinary incontinence and neurogenic detrusor overactivity. However, the information regarding the effects of SOL on membrane ionic currents is largely uncertain, despite its clinically wide use in patients with those disorders. In this study, the whole-cell current recordings revealed that upon membrane depolarization in pituitary GH$_3$ cells, the exposure to SOL concentration-dependently increased the amplitude of M-type K$^+$ current (I$_{K(M)}$) with effective EC$_{50}$ value of 0.34 µM. The activation time constant of I$_{K(M)}$ was concurrently shortened in the SOL presence, hence yielding the K$_D$ value of 0.55 µM based on minimal reaction scheme. As cells were exposed to SOL, the steady-state activation curve of I$_{K(M)}$ was shifted along the voltage axis to the left with no change in the gating charge of the current. Upon an isosceles-triangular ramp pulse, the hysteretic area of I$_{K(M)}$ was increased by adding SOL. As cells were continually exposed to SOL, further application of acetylcholine (1 µM) failed to modify SOL-stimulated I$_{K(M)}$; however, subsequent addition of thyrotropin releasing hormone (TRH, 1 µM) was able to counteract SOL-induced increase in I$_{K(M)}$ amplitude. In cell-attached single-channel current recordings, bath addition of SOL led to an increase in the activity of M-type K$^+$ (K$_M$) channels with no change in the single channel conductance; the mean open time of the channel became lengthened. In whole-cell current-clamp recordings, the SOL application reduced the firing of action potentials (APs) in GH$_3$ cells; however, either subsequent addition of TRH or linopirdine was able to reverse SOL-mediated decrease in AP firing. In hippocampal mHippoE-14 neurons, the I$_{K(M)}$ was also stimulated by adding SOL. Altogether, findings from this study disclosed for the first time the effectiveness of SOL in interacting with K$_M$ channels and hence in stimulating I$_{K(M)}$ in electrically excitable cells, and this noticeable action appears to be independent of its antagonistic activity on the canonical binding to muscarinic receptors expressed in GH$_3$ or mHippoE-14 cells.

Keywords: solifenacin (Vesicare$^®$); M-type K$^+$ current; current kinetics; voltage-dependent hysteresis; M-type K$^+$ channel; pituitary cell; hippocampal neuron

1. Introduction

Solifenacin (Vesicare$^®$, SOL), a member of isoquinolines (Figure 1), has been viewed as an oral anticholinergic (i.e., a competitive muscarinic [M$_1$ and M$_3$] receptor antagonist) and antispasmodic agent used to treat the symptoms of overactive bladder, neurogenic detrusor overactivity, or urinary incontinence [1–8]. It has been reported to be a muscarinic (M$_2$ and M$_3$) receptor antagonist that has anticholinergic effects such as relaxation of the detrusor muscle in urinary bladder [9].
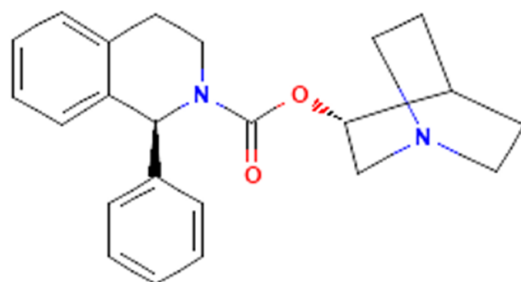
Figure 1. Chemical structure of solifenacin (Vesicare®, [(3R)-1-azabicyclo [2.2.2]octan-3-yl] (1S)-1-phenyl-3,4-dihydro-1H-isoquinoline-2-carboxylate, 2(1H)-isoquinolinecarboxylic acid, 3,4-dihydro-1-phenyl-,1-azabicyclo(2.2.2.)oct-3-yl ester, (R-(R*,S*))-905, quinculidin-3′-yl-1-phenyl-1,2,3,4-tetrahydroisoquinoline-2-carboxylate).

Earlier clinical investigations have revealed the efficacy and safety of the antimuscarinic, solifenacin (SOL), for treating patients with overactive bladder or neurogenic detrusor overactivity [1–5,7,8,10–19]. However, recent evidence has been reported showing that the treatment with SOL could be closely linked to an increased risk of the impairment in cognitive functions [20–31]. Therefore, it is pertinent to reappraise the mechanism of SOL actions on electrical behaviors in varying excitable cells, given that its growing clinical use occurs [6,32].

Many types of anterior pituitary cells have been previously demonstrated to secrete acetylcholine [33]. Earlier studies have also revealed that pituitary GH_3 cells could exhibit the activity of muscarinic receptors and that muscarinic agonists were able to inhibit hormonal secretion through a reduction in intracellular cyclic AMP [33–40]. In these cells, the binding of acetylcholine to M_2-muscarinic receptor might induce a weak stimulation on the hydrolysis of phosphatidylinositol 4,5-bisphosphate [41]. The binding of acetylcholine to muscarinic receptors in GH_3 cells was also reported to activate the activity of G protein-coupled K^+ channels directly [42,43] and to inhibit voltage-gated Ca^{2+} currents [44]. Whether SOL could perturb the electrical activities directly or indirectly through its binding of acetylcholine to muscarinic receptors in pituitary cells is uncertain.

The KCNQ2, KCNQ3, or KCNQ5 gene is viewed to encode the core subunit of $K_V7.2$, $K_V7.3$, or $K_V7.5$ channel, respectively. The enhanced activity of this family of voltage-gated K^+ channels (KCNQx or K_M channels) can generate the macroscopic M-type K^+ current ($I_{K(M)}$), which is biophysically characterized by current activation in response to low-threshold voltage [45]. Once being activated, this type of K^+ currents can be sensitive to block by linopirdine and it is demonstrated to exhibit a slowly activating and deactivating property [46–51]. Alternatively, targeting $I_{K(M)}$ has been noticeably viewed as an adjunctive regimen for the management of various neurological, smooth muscle, or endocrine disorders closely linked to membrane hyperexcitability, which include cognitive dysfunction, epilepsy, and over-active bladder [47,52–55]. However, to our knowledge, how and whether this agent can interact directly with K_V channels to modify the amplitude and gating of voltage-gated K^+ currents (e.g., M-type K^+ current) remain largely unknown.

Therefore, in terms of the considerations stated above, in the current study, we decided to explore the possible perturbations of SOL on $I_{K(M)}$ in pituitary GH_3 cells and mouse mHippoE-14 hippocampal neurons. Findings from the present observations enable us to reflect that the $I_{K(M)}$ inherent in different cell types could be an additional and yet non-canonical target through which SOL can act to govern the functional activities of the cells involved, presuming that similar in vitro or in vivo findings occur. It thus merit attention that the stimulation of $I_{K(M)}$ and the antagonistic effect on the binding to muscarinic receptors may potentially converge to act on the functional activities of neurons, and neuroendocrine or endocrine cells.

2. Results

2.1. Effect of SOL on the M-Type K$^+$ Current ($I_{K(M)}$) Measured from GH$_3$ Cells

For the first stage of experiments, we intended to determine the possible effect of SOL on the amplitude and kinetics of $I_{K(M)}$ identified in these cells. In attempts to measure the magnitude of $I_{K(M)}$, we kept cells bathed in high-K$^+$, Ca^{2+}-free solution which contained 1 μM tetrodotoxin (TTX), and the recording pipette was backfilled with a K$^+$-containing (145 mM) solution. When the whole-cell configuration was established, we held the examined cell in voltage-clamp mode at the level of −50 mV and a 1-sec depolarizing command voltage to −10 mV was thereafter applied to it. Under these experimental conditions, a specific population of K$^+$ currents with a slowly activating and deactivating property was robustly evoked and it has been thus viewed as an $I_{K(M)}$ [48,49,51,56]. This type of $I_{K(M)}$ found in pituitary lactotrophs including GH$_3$ cells has been demonstrated to be sensitive to be blocked by thyrotropin releasing hormone (TRH) [48,57]. As demonstrated in Figure 2A,B, the $I_{K(M)}$ in response to step depolarization from −50 to −10 mV was sensitive to inhibition by 10 μM linopirdine (Lino) or 1 μM TRH, while the presence of 10 μM naringenin (NGEN) or 10 μM ML213 increased current amplitude. NGEN or ML213 was previously reported to be an activator of $I_{K(M)}$ [58,59]. Of particular interest, one minute after GH$_3$-cell exposure to SOL, the amplitude of $I_{K(M)}$ upon 1-sec membrane depolarization from −50 to −10 mV progressively became increased together with a concurrent decrease in the activation time constant (τ_{act}) of the current (Figure 3A). For example, the addition of 0.3 or 1 μM SOL increased $I_{K(M)}$ amplitude to 56 ± 7 pA ($n = 8$, $p < 0.05$) or 77 ± 9 pA ($n = 8$, $p < 0.05$), respectively, from control value of 36 ± 6 pA ($n = 8$). Concomitantly, the presence of 0.3 or 1 μM SOL also reduced the τ_{act} value to 89.1 ± 12.5 msec or 56.7 ± 10.1 msec, respectively, from control value of 123.5 ± 16.8 msec ($n = 8$). After SOL was removed, current amplitude was returned to 39 ± 7 pA ($n = 7$).
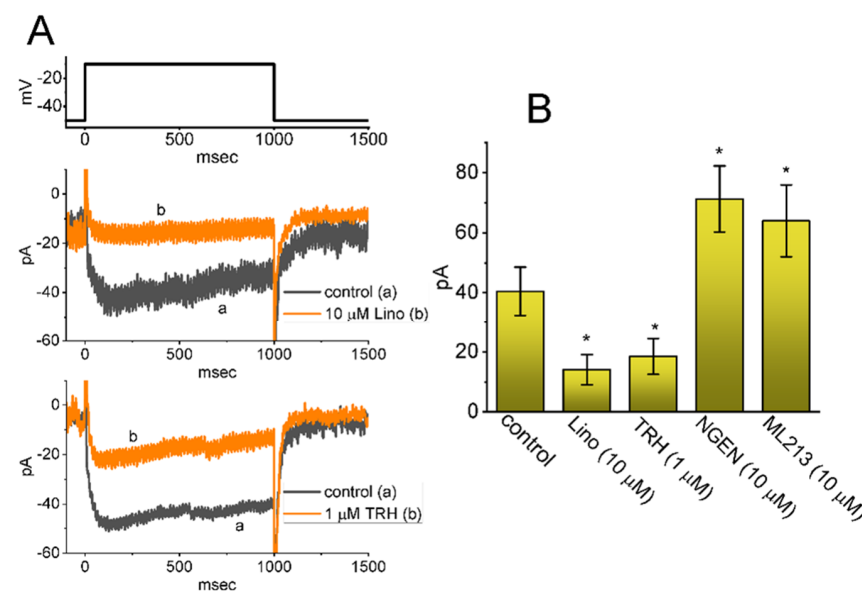
Figure 2. Effect of linopirdine (Lino), thyrotropin releasing hormone (TRH), naringenin (NGEN) or ML213 on M−type K$^+$ current ($I_{K(M)}$) recorded from pituitary tumor (GH$_3$) cells. These experiments were performed in cells which were kept bathed in high−K$^+$, Ca^{2+}−free solution containing 1 μM TTX and 0.5 mM CdCl$_2$, and we then backfilled the recording electrode by using K$^+$−containing (145 mM) solution. (**A**) Representative current traces obtained in the control period (a's) or during exposure (b's) to 10 μM Lino (upper part) or 1 μM TRH (lower part). The uppermost part shows the voltage−clamp protocol used. (**B**) Summary bar graph showing effects of Lino, TRH, NGEN, or ML213 on the amplitude of $I_{K(M)}$ in GH$_3$ cells (mean ± SEM; $n = 7$ for each bar). Current amplitude was measured at the end of depolarizing pulse from −50 to −10 mV. Statistical analysis was made by ANOVA−1 ($p < 0.05$). * Significantly different from control ($p < 0.05$).
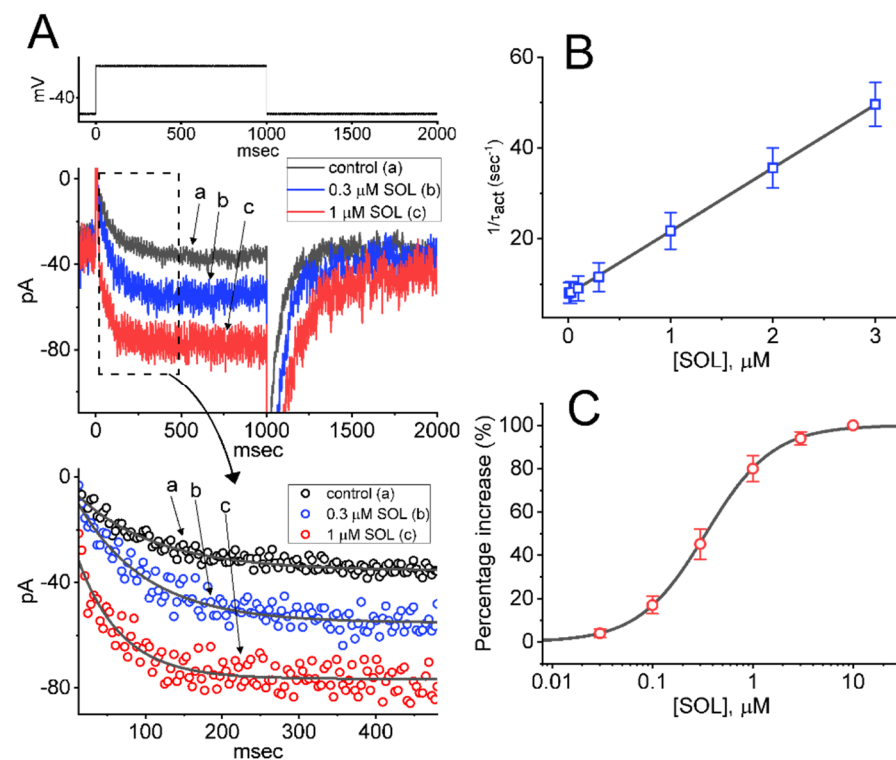
Figure 3. Effect of SOL on $I_{K(M)}$ recorded from GH_3 cells. This set of experiments was undertaken in cells which was kept bathed in high$-K^+$, $Ca^{2+}-$free solution containing 1 μM TTX and 0.5 mM $CdCl_2$, and we backfilled the recording electrode by using K^+-containing (145 mM) solution. (**A**) Representative $I_{K(M)}$ traces obtained in the control period (i.e., SOL was not present; a) and during cell exposure to 0.3 μM SOL (b) or 1 μM SOL (c). The uppermost part denotes the voltage−clamp protocol applied, while the lower part shows the activation time courses of $I_{K(M)}$ taken in the absence (a) and presence of 0.3 μM SOL (b) or 1 μM SOL (c). Current traces in the bottom panel show an expanded record from the dashed box in the top panel, and their trajectories taken from (A) was well fitted by a single exponential (indicated in smooth gray line). Data points (indicated in open circles) with or without the addition of SOL are reduced by 20. (**B**) Kinetic estimate of SOL−stimulated $I_{K(M)}$ identified in GH_3 cells (mean ± SEM; *n* = 8 for each point). The reciprocal of activation time constant of $I_{K(M)}$ ($1/\tau_{act}$) derived from exponential fit of the $I_{K(M)}$ trajectory was collated and linearly plotted against the SOL concentration (gray straight line). Forward (k_{+1}^*) or backward (k_{-1}) rate constant for the binding scheme, derived from the slope and the *y*−axis of the interpolated line was estimated to be 13.962 $sec^{-1}μM^{-1}$ or 7.672 sec^{-1}, respectively; thereafter, the K_D value (k_{-1}/k_{+1}^* = 0.55 μM) was yielded. (**C**) Concentration−dependent relationship of SOL effect on $I_{K(M)}$ activated by 1−sec long membrane depolarization (mean ± SEM; *n* = 8 for each point). Current amplitude was measured at the end−pulse of each depolarizing step from −50 to −10 mV with a duration of 1 sec. The sigmoidal curve (gray line) indicates the goodness of fit to the Hill equation, as stated in Materials and Methods.

Because the $I_{K(M)}$ activation in response to long-last step depolarization tends to be shortened, our next goal was to determine the kinetics of *SOL*-stimulated currents seen in GH_3 cells. As demonstrated in Figure 3B, as cells were rapidly depolarized from −50 to −10 mV with a duration of 1 sec, it was noticed that exposure to *SOL* resulted in a reduction in the τ_{act} value in a concentration-dependent manner. This finding can thus be interpreted to reflect that the stimulatory effect of *SOL* on $I_{K(M)}$ seen in GH_3 cells is explained by the state-dependent activation in situations where the molecule can preferentially bind to

the open state (conformation) of the M-type K^+ (K_M) channel, on the assumption of the first-order reaction scheme:

$$C \underset{\beta}{\overset{\alpha}{\rightleftarrows}} O \underset{k_{-1}}{\overset{k^*_{+1}\cdot[SOL]}{\rightleftarrows}} O\cdot[SOL] \tag{1}$$

or

$$\frac{dC}{dt} = \beta \times O - \alpha \times C$$
$$\frac{dO}{dt} = \alpha \times C + k_{-1} \times O\cdot[SOL] - O \times \left(\beta + k^*_{+1}\cdot[SOL]\right)$$
$$\frac{dO\cdot[SOL]}{dt} = k^*_{+1}\cdot[SOL] \times O - k_{-1} \times O\cdot[SOL]$$

where α or β represents kinetic constant for the opening or closing of K_M channel, respectively; and k^*_{+1} or k_{-1} is that for forward (on-) or reverse (off-) rate constant of the *SOL* binding, respectively. "*C*", "*O*", or "*O* [*SOL*]" denotes the closed, open, or open [*SOL*] state of the channel, respectively. Forward or reverse rate constant (k^*_{+1} or k_{-1}) in this reaction was evaluated from the τ_{act} values for *SOL*-stimulated modification in the trajectory of $I_{K(M)}$ activation, as described under the Materials and Methods (Figure 3B). The value of k^*_{+1} or k_{-1} obtained from eight different cells was consequently determined to be 13.962 sec^{-1} μM^{-1} or 7.672 sec^{-1}, respectively; thereafter, the value of dissociation constant ($K_D = k_{-1}/k^*_{+1}$) was calculated to be 0.55 μM.

The relationship between the *SOL* concentration and the percentage increase of $I_{K(M)}$ was determined and thereafter constructed. In these experiments, each examined cell was held at -50 mV and the depolarizing step from -50 to -10 mV with a duration of 1 sec was delivered to it, and the $I_{K(M)}$ amplitudes during exposure to different concentrations (0.3–10 μM) of *SOL* were measured at the end of depolarizing step. As illustrated in Figure 3C, *SOL* increased $I_{K(M)}$ amplitude in a concentration-dependent fashion. By use of a non-linear least-squares fit to the experimental data, the EC_{50} value required for the stimulatory effect of *SOL* on $I_{K(M)}$ in GH_3 cells was calculated to be 0.34 μM, a value that was noticeably similar to the K_D value estimated above. As such, these emerging data reflect that SOL alone is able to render $I_{K(M)}$ to be sensitive to stimulation attainable in these cells, which appears to be unlinked to its binding to muscarinic receptors.

2.2. Comparison in $I_{K(M)}$ Amplitudes Caused by the Presence of SOL, SOL plus Acetylcholine (ACh), SOL plus Iberiotoxin (Iber), SOL plus Apamin (Apa), SOL plus Tolbutamide (TLB), SOL plus Chlorotoxin (ChTx), SOL plus Linopirdine (Lino), or SOL plus Thyrotropin Releasing Hormone (TRH)

We continued to examine whether SOL-stimulated $I_{K(M)}$ in GH_3 cells could be modified by further application of acetylcholine, iberiotoxin, apamin, tolbutamide, chlorotoxin, linopirdine, or thyrotropin releasing hormone. The muscarinic receptor in GH_3 cells can be activated by acetylcholine [42,43], while iberiotoxin or apamin is an inhibitor of large- or small-conductance Ca^{2+}-activated K^+ channels, respectively, whereas tolbutamide is reported to suppress ATP-sensitive K^+ channel. Chlorotoxin is known to suppress the activity of Cl^- channels, while Lino or TRH is an inhibitor of $I_{K(M)}$ in GH_3 cells [48–51]. In the examined cells bathed in high-K^+, Ca^{2+}-free solution, the potential was held at -50 mV and the depolarizing step from -50 to -10 with a duration of 1 sec was applied to the cell. Summary bar graph demonstrated in Figure 4 revealed that cell exposure to 1 μM SOL increased $I_{K(M)}$ amplitude and that neither further addition of acetylcholine (10 μM), iberiotoxin (200 nM), apamin (200 nM), tolbutamide (10 μM), nor chlorotoxin (1 μM) resulted in any adjustments in SOL-stimulated $I_{K(M)}$, while that of Lino or TRH was able to reverse the stimulation of $I_{K(M)}$ caused by SOL. The results indicate that the $I_{K(M)}$ amplitude stimulated by SOL seen in GH_3 cells is unlinked to its effects on the activity of large- or small-conductance Ca^{2+}-activated K^+ channels or on that of ATP-sensitive K^+ channels, and that its stimulatory effect on $I_{K(M)}$ is unable to be adjusted by further application of acetylcholine.
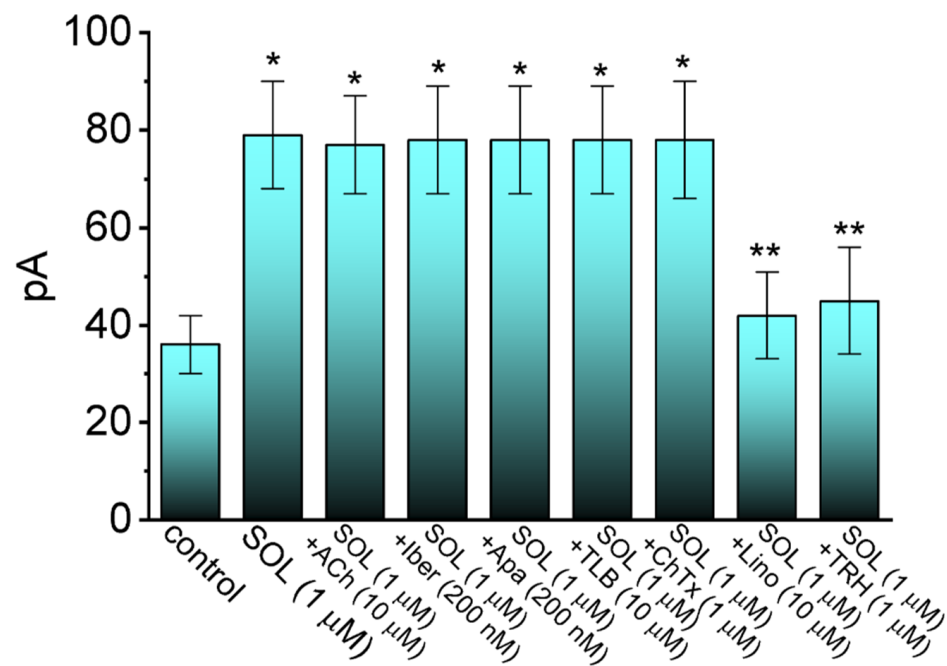
Figure 4. Effect of SOL, SOL plus acetylcholine (ACh), SOL plus iberiotoxin (Iber), SOL plus apamin (Apa), SOL plus tolbutamide (TLB), SOL plus chlorotoxin (ChTx), SOL plus Lino, or SOL plus TRH on the amplitude of $I_{K(M)}$. In these experiments, we bathed GH$_3$ cells in high-K$^+$, Ca^{2+}-free solution and the recording electrode was filled with K$^+$-enriched (145 mM) solution. Current amplitude was measured at the end of the depolarizing step from -50 to -10 mV. Each bar represents the mean $\pm$ SEM ($n = 7$). * Significantly different from controls ($p < 0.05$) and ** significantly different from SOL (1 μM) alone group ($p < 0.05$).

2.3. Current-Voltage (I-V) Relationship and Steady-State Activation Curve of $I_{K(M)}$ in the Absence and Presence of SOL

We next studied whether the presence of SOL can modify the amplitude of $I_{K(M)}$ measured at different level of membrane potentials. The averaged *I-V* relationship of $I_{K(M)}$ with or without the addition of SOL (1 μM) is illustrated in Figure 5A. The current amplitude was significantly increased as the membrane potential was less negative to -30 mV, and the magnitude of SOL-stimulated current at the level of -10 mV was noted to be greater than that at -20 mV. The relationship of $I_{K(M)}$ conductance versus membrane potential gained in the control period (i.e., SOL was not present) and during cell exposure to SOL (1 μM) was collated (Figure 5B). The smooth sigmoidal curve derived from data sets was reliably fitted with a modified Boltzmann function (described under Materials and Methods). That is, the value of $V_{1/2}$ or q taken in the control period was -17.4 ± 2.1 mV ($n = 8$) or 6.4 ± 0.9 e ($n = 8$), respectively, while that in the presence of 1 μM SOL was -28.2 ± 2.2 mV ($n = 8$) or 6.1 ± 0.9 e ($n = 8$), respectively. The data enable us to reflect that, in addition to increasing $I_{K(M)}$ conductance, the addition of SOL was capable of producing a leftward shift along the voltage axis, albeit with no marked change in the gating charge of the current.
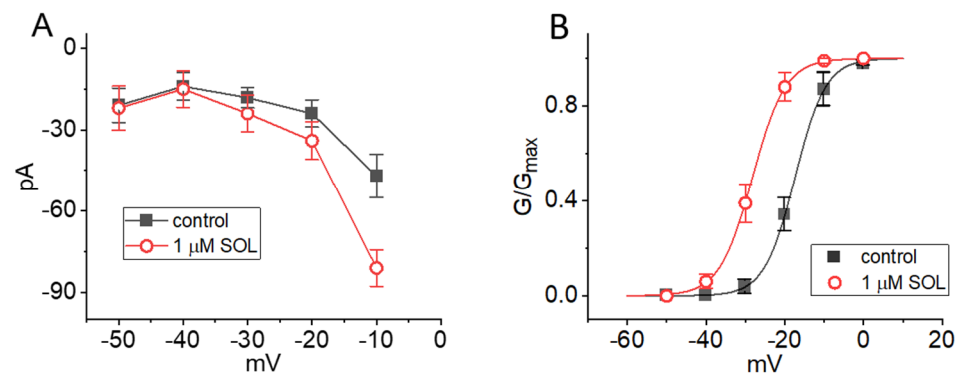
Figure 5. Effect of SOL on the current-voltage (*I-V*) relationship (**A**) and activation curve (**B**) of $I_{K(M)}$ identified in GH$_3$ cells. In these experiments, the examined cell was held at −50 mV and the voltage pulses ranging between −50 and 0 mV in 10-mV step were applied to it. (**A**) Averaged *I-V* relationship of $I_{K(M)}$ taken in the absence (■) and presence (○) of 1 μM SOL (mean ± SEM; *n* = 8 for each point). Each data point was taken at the end-point of each voltage pulse. (**B**) Activation curve (i.e., normalized conductance versus membrane voltage) of $I_{K(M)}$ obtained in the control period (■) and during exposure (○) to 1 μM SOL (mean ± SEM; *n* = 8 for each point). The smooth continuous lines give best fit to a modified Boltzmann equation as stated in Materials and Methods. Of note, a leftward shift along the voltage axis in the activation curve of $I_{K(M)}$ recorded from GH$_3$ cells is illustrated in the presence of 1 μM SOL, despite no perturbation in the apparent gating charge of the current. The statistical analyses in (**A**) and (**B**) were undertaken by ANOVA-2 for repeated measures, *p* (factor 1, groups among data taken at different level of membrane potentials) < 0.05, *p* (factor 2, groups between the absence and presence of SOL) < 0.05, *p* (interaction) < 0.05, followed by post-hoc Fisher's least-significance difference test (*p* < 0.05).

2.4. Effect of SOL on Voltage-Dependent Hysteresis (V_{hys}) of $I_{K(M)}$ Activated by Long Isosceles-Triangular Ramp Pulse

The V_{hys} of membrane ionic currents (i.e., a lag in the current amplitude as the linear voltage ramp is changed in the opposite direction) has been recently noticed with an impact on the electrical signal events of varying excitable cells [51,60–66]. In other words, V_{hys} behavior is thought to dynamically adjust the voltage sensitivity and kinetics to optimize channel function for appropriately matching its physiological or pathophysiological role in regulation of AP firing [62,63,65]. Toward this goal, we continued to determine how the presence of SOL might adjust the V_{hys} strength of $I_{K(M)}$. In this separate set of experiments, as soon as the whole-cell configuration was achieved, we maintained the examined cell in voltage clamp at −50 mV, and a long-lasting upright isosceles-triangular ramp pulse with a duration of 2 sec at voltages between −45 and +5 mV (i.e., a ramp slope of ±50 mV/sec) was digitally created and, through DA conversion via Digidata 1440A device, thereafter, delivered to the examined cell at a rate of 0.025 Hz. Of notice, as demonstrated in Figure 6, the $I_{K(M)}$ trajectories elicited in response to the forward upsloping (i.e., voltage change from −45 to +5 mV) ramp pulse and by the backward downsloping (i.e., the change from +5 to −45 mV) as a function of time (as indicated by the dashed arrows in Figure 6A) were markedly distinguishable between these two limbs. In other words, the $I_{K(M)}$ amplitude activated by the upsloping (forward or ascending) limb of the triangular voltage ramp was demonstrated to be smaller than that by the downsloping (backward or descending) end of the ramp. These observations led us to indicate that there was a V_{hys} phenomenon ranging between −45 and −5 mV for this type of recorded currents in GH$_3$ cells.
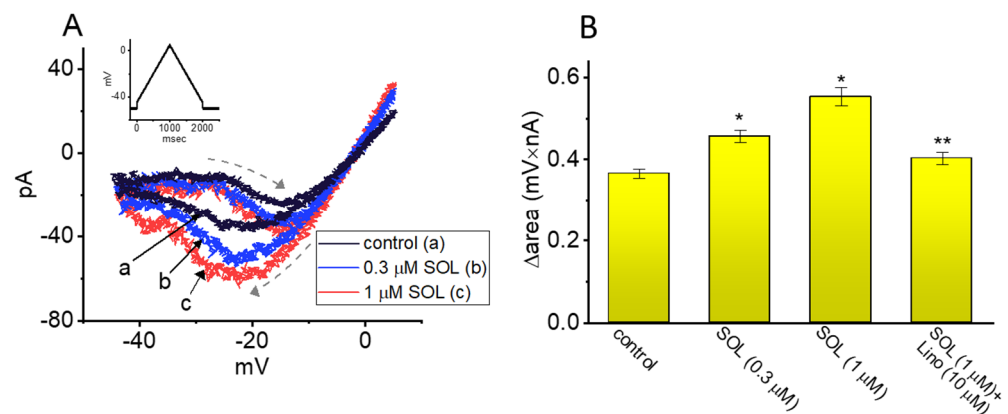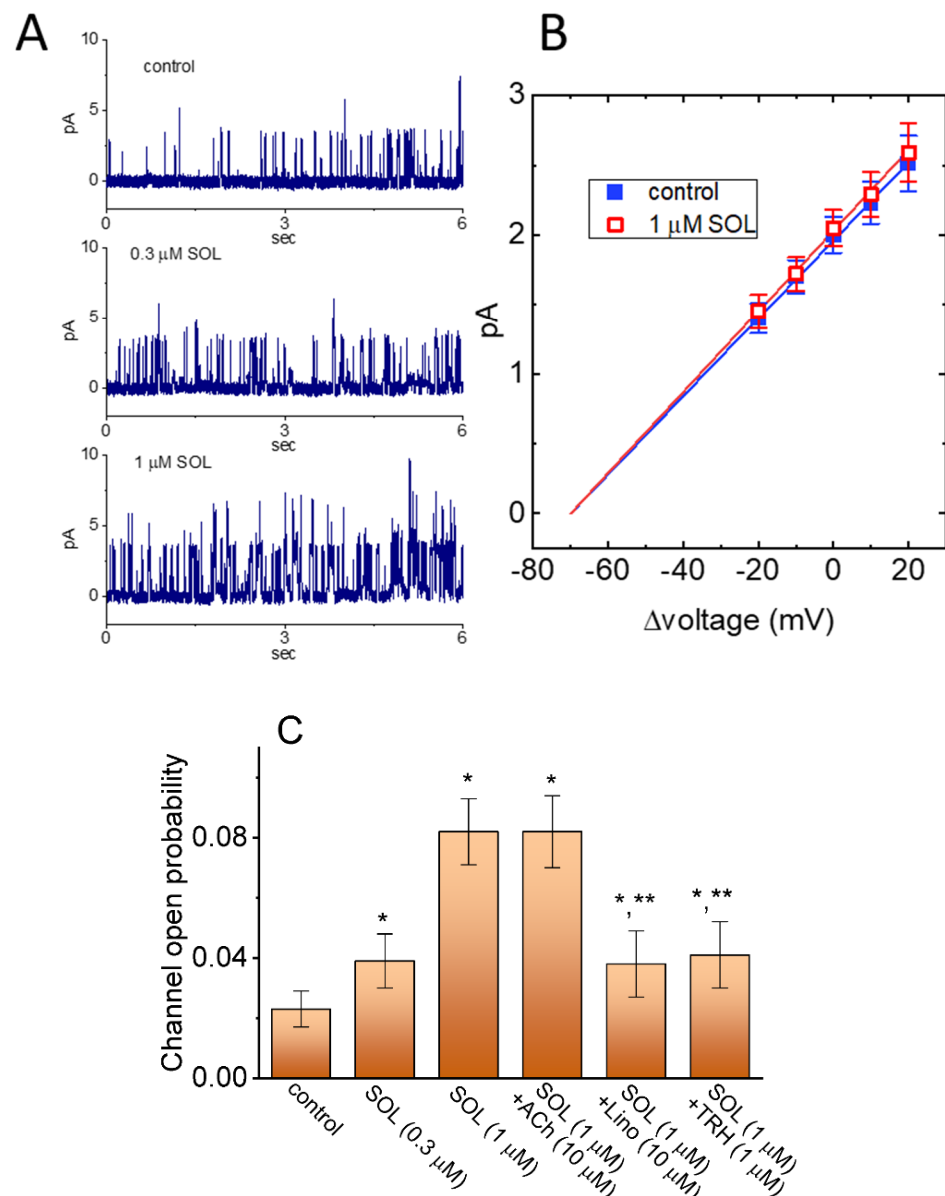
Figure 6. Stimulatory effect of SOL on voltage−dependent hysteresis (V_{hys}) of $I_{K(M)}$ in GH$_3$ cells. This set of experiments was conducted with an isosceles−triangular ramp pulse. (**A**) Representative current traces activated in response to isosceles−triangular ramp pulse with a duration of 2 sec obtained in the control period (black line, a) and during cell exposure to 0.3 μM SOL (blue line, b) or 1 μM SOL (red line, c). The dashed arrows indicate the distinctive patterns of current trajectory by which time passes as the ramp pulse is applied. The voltage−clamp ramp pulse is illustrated in inset at the left upper corner. (**B**) Hysteretic area (i.e., Δarea) of $I_{K(M)}$ V_{hys} gained in control period (i.e., SOL was not present) or during exposure to SOL and SOL plus linopirdine (Lino). The area encircled by current amplitudes activated in the ascending and descending limb at the voltages between −45 and 0 mV was calculated. Each bar indicates the mean ± SEM ($n = 7$ for each bar). Data analysis was performed by ANOVA−1 ($p < 0.05$). * Significantly different from control ($p < 0.05$) and ** significantly different from SOL (1 μM) alone group ($p < 0.05$).

In this study, we continued to quantify the V_{hys} strength of $I_{K(M)}$ on the basis of the area encircled by the curvilinear trajectory in response to the upsloping and downsloping direction in ramp voltage. Figure 6B illustrates a summary of the area under the curve (i.e., Δarea) between the forward and backward currents activated in response to a 2-sec isosceles-triangular ramp pulse. Of notice, when the whole-cell $I_{K(M)}$ was identified, the addition of 0.3 or 1 μM SOL actually increased the area up to 1.2- or 1.5-fold, respectively, while the subsequent application of 10 μM linopirdine, an inhibitor of K_M channels, markedly attenuated SOL-induced increase in the area by around 30%. It is conceivable, therefore, that the V_{hys} of $I_{K(M)}$ in these cells can be augmented by the presence of SOL.

2.5. Stimulatory Effect of SOL on the Activity of M-Type K⁺ (K_M) Channels in GH$_3$ Cells

The SOL-induced raise in whole-cell $I_{K(M)}$ stated above could be due to either changes in channel open probability, single-channel amplitude, gating kinetics of the K_M channels, or in any combinations. Such reasons thus urged us to assess the single-channel activities of the channels residing in GH$_3$ cells. In this stage of cell-attached current recordings, we bathed cells in high-K⁺, Ca²⁺-free solution and the recording electrode used was filled up with low-K⁺ (5.4 mM) solution. As demonstrated in Figure 7, as the examined cell was held at +20 mV relative to the bath, the activity of single-K_M channels was robustly detected [51,56,66]. One minute after bath application of SOL, the channel open probability was markedly raised. For example, at the level of +20 mV relative to the bath, the presence of 1 μM SOL significantly increased the probability of channel openings from 0.023 ± 0.006 to 0.082 ± 0.012 ($n = 7$, $p < 0.01$); conversely, no appreciable modification in the single-channel amplitude was shown in its presence (28 ± 2 pS [control] versus 29 ± 2 pS [in the presence of SOL]; $n = 7$, $p > 0.05$). Meanwhile, the mean open time of K_M channels in its presence was appreciably increased to 5.2 ± 1.1 msec ($n = 7$, $p < 0.05$) from a control value of 2.8 ± 0.9 msec ($n = 7$). Furthermore, as cells were continually exposed to SOL, subsequent addition of Lino (10 μM) or TRH (1 μM) could attenuate SOL-stimulated channel activity, while that of acetylcholine (10 μM) failed to influence it. However, no detectable change in

single-channel conductance of K_M channels was observed, although the mean open time of the channel lengthened as well as the channel open probability was elevated.

Figure 7. Stimulatory effect of SOL on the activity of M−type K^+ (K_M) channels in recorded GH_3 cells. In this set of cell−attached current recordings, we bathed cells in high−K^+, Ca^{2+}−free solution, while the recording electrode was filled up with low−K^+ (5.4 mM) solution. (**A**) Representative single K_M−channel activity obtained in the control period (upper) and during cell exposure to 0.3 μM SOL (middle) or 1 μM SOL (lower). The examined cells were maintained at +20 mV relative to the bath, and the upward deflection indicates the opening event of the channel. (**B**) Averaged *I-V* relationships of single-channel K_M currents between the absence (■) and presence (□) of 1 μM SOL (mean ± SEM; *n* = 8 for each point). Notably, no appreciable difference in single−channel conductance of K_M channels is depicted in the presence of 1 μM SOL. (**C**) Summary bar graph showing effect of SOL, SOL plus acetylcholine (ACh), SOL plus linopirdine (Lino), or SOL plus thyrotropin releasing hormone (TRH) on the probabilities of K_M-channel openings (mean ± SEM; *n* = 7 for each bar). Channel activity was measured at the level of +20 mV relative to the bath. Data analysis was performed by ANOVA−1 (*p* < 0.05). * Significantly different from control (*p* < 0.05) and ** significantly different from SOL (1 μM) alone group (*p* < 0.05).

2.6. Effect of SOL on Spontaneous Action Potentials (APs) Recorded from GH$_3$ Cells

For another stage of the experiments, the measurements were repurposed to whole-cell potential recordings, in attempts to assess the possible perturbations of SOL on the firing frequency of APs found in these cells. For this stage of measurements, we suspended cells to be bathed in normal Tyrode's solution containing 1.8 mM CaCl$_2$, the recording pipet was filled with K$^+$-enriched solution, and whole-cell current-clamp configuration was carried out. As demonstrated in Figure 8, one minute after cell exposure to 0.3 or 1 μM SOL, the firing rate (i.e., spikes/sec) of spontaneous APs was noticeably diminished in combination with concurrent membrane hyperpolarization. For example, the presence of SOL at a concentration of 1 μM overly decreased the firing frequency of spontaneous APs to 0.47 ± 0.03 Hz (n= 8, $p < 0.05$) from a control value of 1.10 ± 0.05 Hz ($n = 8$). Moreover, during continued exposure to SOL, subsequent addition of TRH (1 μM) or Lino (10 μM) was able to reverse SOL-mediated inhibition of spontaneous APs effectively. It is likely, therefore, that SOL-mediated decrease in firing frequency of spontaneous APs is mostly mediated through its stimulation of I$_{K(M)}$ identified in GH$_3$ cells.
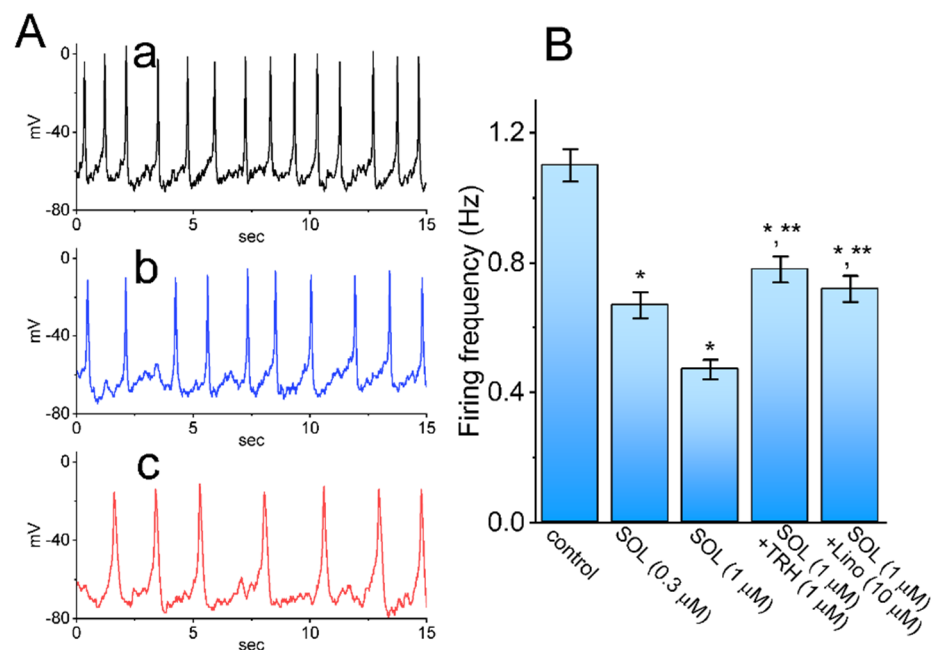

Figure 8. Effect of SOL on spontaneous action potentials (APs) recorded from GH$_3$ cells. Whole-cell current-clamp potential recording was carried out in this series of measurements. (**A**) Representative potential traces obtained in the control period (a) and during cell exposure to 0.3 μM SOL (b) or 1 μM SOL (c). (**B**) Summary bar graph showing effect of SOL, SOL plus TRH and SOL plus Lino on firing frequency of APs (mean ± SEM; $n = 8$ for each bar). Data analysis was made by ANOVA-1 ($p < 0.05$). * Significantly different from control ($p < 0.05$) and ** significantly different from SOL (1 μM) alone group ($p < 0.05$).

2.7. Stimulatory Effect of SOL on I$_{K(M)}$ Present in mHippoE-14 Neurons

Evidence has recently accumulated that the treatment with SOL could be linked to an increased risk of the impairment in cognitive functions [20–31]. Earlier reports have also reported the ability of this drug to influence the muscarinic activity in cerebral cortex and hippocampus [67,68]. For these reasons, we further assessed the possible adjustments of SOL on I$_{K(M)}$ in hippocampal mHippoE-14 neurons. This cell line tends to be a homogenous population and it is known to possess the characteristics of embryonic hippocampal neurons valuable for the investigations on different types of neurological disorders [56,69–71]. In this series of experiments, we bathed mHippoE-14 cells in high-K$^+$, Ca^{2+}-free solution which contained 1 μM TTX, and we filled up the recording electrodes by using K$^+$-enriched (145 mM) solution. As whole-cell configuration was established,

the examined cell was held at -50 mV in voltage-clamp mode and the depolarizing pulse to -10 mV with a duration of 1 sec was delivered to it. As shown in Figure 9 as cells were acutely exposed to different concentrations of SOL, the amplitude of $I_{K(M)}$ activated by such voltage-clamp protocol progressively rose. For example, the presence of 1 μM SOL augmented $I_{K(M)}$ amplitude from 28 ± 4 to 65 ± 8 pA ($n = 7$, $p < 0.05$); and, after removal of SOL, current amplitude was returned to 30 ± 5 pA ($n = 7$). In the continued presence of 1 μM SOL, further application of Lino (μM) attenuated SOL-stimulated $I_{K(M)}$, as demonstrated by an appreciable reduction of $I_{K(M)}$ amplitude to 36 ± 5 pA ($n = 7$, $p < 0.05$). Therefore, it is plausible to assume that indistinguishable from those identified above in GH$_3$ cells, $I_{K(M)}$ present in mHippoE-14 neurons, to which $I_{K(M)}$ confers excitability, is subject to stimulation by SOL.
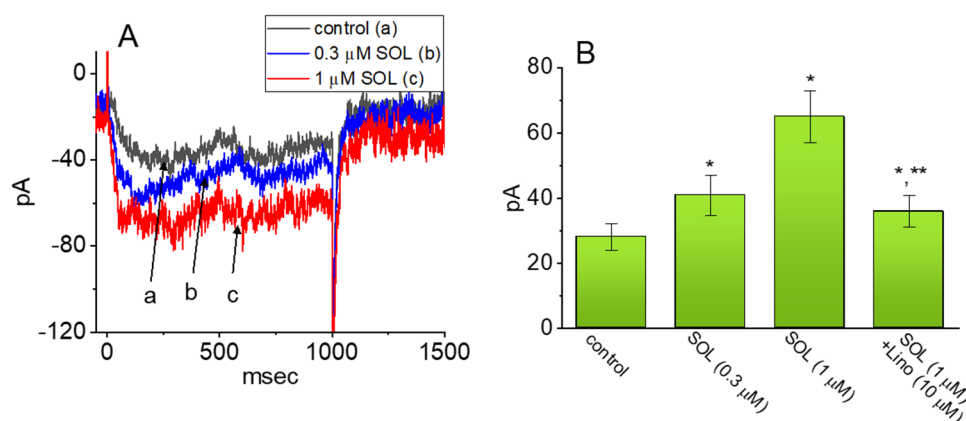
Figure 9. Stimulatory effect of SOL on $I_{K(M)}$ recorded from mouse hippocampal mHippoE-14 neurons. In this set of whole-cell voltage-clamp experiments, cells were bathed in high-K$^+$, Ca^{2+}-free solution, the recording pipette used was filled up with a K$^+$-enriched (145 mM) solution, and the examined cells were depolarized from -50 to -10 mV with a duration of 1 sec. (**A**) Representative current traces obtained in the control period (a) and in the presence of 0.3 μM SOL (b) or 1 μM SOL (c). (**B**) Summary bar graph showing effect of SOL and SOL plus linopirdine (Lino) on the amplitude of $I_{K(M)}$ in mHippoE-14 cells (mean $\pm$ SEM; $n = 7$ for each bar). Current amplitude was measured at the end-point of the depolarizing command from -50 to -10 mV. Data analysis was performed by ANOVA-1 ($p < 0.05$). * Significantly different from control ($p < 0.05$) and ** significantly different from SOL (1 μM) alone group ($p < 0.05$). Of notice, the presence of SOL exercises a stimulatory effect on $I_{K(M)}$, and subsequent addition of linopirdine attenuates SOL-mediated stimulation of current amplitude.

3. Discussion

The salient findings noticed in the current investigations are as follows: (a) In pituitary GH$_3$ cells, during exposure to SOL, the $I_{K(M)}$ amplitude upon long membrane depolarization was concentration-dependently increased and the activation time course of the current concurrently became shortened; (b) the EC$_{50}$ or K$_D$ value of SOL-stimulated $I_{K(M)}$ was calculated to be 0.34 or 0.55 μM, respectively; (c) there is a leftward shift of the steady-state activation curve of $I_{K(M)}$ in its presence; (d) the V$_{hys}$ area of $I_{K(M)}$ activated by isosceles-triangular ramp pulse increased during cell exposure to SOL; (e) the K$_M$-channel activity was elevated by adding SOL; however, no change in single-channel conductance of the channel was detected; (f) under current-clamp conditions, the firing frequency of spontaneous APs was measured to be appreciably decreased in the presence of this drug; and (g) the $I_{K(M)}$ inherently in hippocampal mHippoE-14 neurons was also subject to stimulation by SOL. Altogether, regardless of the unresolved detailed ionic mechanism of its actions on K$_M$ (or KCNQx) channels, the present results provide an unanticipated and yet non-canonical ionic mechanisms through which the SOL molecule can interact with K$_M$ channels to increase whole-cell $I_{K(M)}$ and, consequently, to diminish the firing rate of spontaneous of APs.

One element that is pertinent to notable findings in this study is that the presence of SOL has the propensity to interact with K_M channels to increase the magnitude of $I_{K(M)}$ as well as to fasten the activation rate of the current during long depolarizing steps. In other words, although the SOL addition was effective at stimulating $I_{K(M)}$, the activation time course of $I_{K(M)}$ evoked by long-step membrane depolarization became raised. The interaction of SOL with K_M channels could also be enhanced by repetitive opening of the channel pore to provide drug access. According to minimal binding scheme, the K_D value was yielded to be 0.55 µM, a value which noticeably bears a similarity to effective EC_{50} value needed for SOL-stimulated $I_{K(M)}$. The steady-state activation curve of $I_{K(M)}$ attained in the SOL presence was also found to be shifted along the voltage axis in a leftward direction (i.e., a more negative potential), with no modifications in the gating charge of the current. The mean open time of K_M channels was also found to become lengthened in its presence. In this regard, it is plausible to assume that the SOL molecule can preferentially bind to the open state of the K_M channel; consequently, the magnitude of $I_{K(M)}$ activated upon long membrane depolarization became elevated during its exposure.

In the present study, the inability of iberiotoxin, apamin, tolbutamide, or chlorotoxin to modify the stimulatory effect on $I_{K(M)}$ caused by the presence of SOL was demonstrated. Iberiotoxin or apamin is viewed to inhibit the activity of large- or small-conductance Ca^{2+}-activated K^+ channels, respectively. Tolbutamide can suppress the activity of ATP-sensitive K^+ channels, and chlorotoxin is a blocker of Cl^- channels. Therefore, it seems unlikely that SOL-mediated stimulation of $I_{K(M)}$ in GH_3 cells is associated with its perturbations on the activities of large- or small-conductance Ca^{2+}-activated K^+ channels, ATP-sensitive K^+ channels, or Cl^- channels, which were reportedly present in GH_3 cells. Additionally, in continued presence of SOL, the subsequent addition of acetylcholine failed to reverse SOL-mediated increase in $I_{K(M)}$ amplitude, reflecting that the stimulatory action on $I_{K(M)}$ would not solely be explained by its competitive binding of acetylcholine to muscarinic receptors in these cells, although GH_3 cells have been previously demonstrated to exhibit the activity of muscarinic receptors [33–40]. Of note, the SOL molecule is structurally similar to tetrahydropyrrolopyrazines demonstrated to activate $I_{K(M)}$ [72], suggesting that 1-phenyl-3,4-dihydro-1H-isoquinoline moiety residing in the molecule is an active site for the binding to the channel.

In accordance with the preceding reports, the V_{hys} phenomenon of $I_{K(M)}$ evoked by the long isosceles-triangular ramp pulse (i.e., the upsloping and downsloping ramp) was revealed in GH_3 cells [73]. The adjustments of such V_{hys} have been recently noticed to serve a role in fine-tuning the activity of ionic channels (e.g., K_M channels) to respond when they are virtually needed [62,63,66,73]. We further determined the possible perturbations of SOL on such dynamic and non-equilibrium properties of $I_{K(M)}$ present in GH_3 cells. The emerging results allowed us to bespeak that the presence of SOL was able to increase the hysteretic strength of the current efficiently (i.e., Δarea in Figure 6) associated with the voltage-dependent activation of instantaneous $I_{K(M)}$. Under such scenario, it is possible that intrinsic changes in the voltage dependence of the voltage-sensing machinery in K_M (KCNQx) channels, namely voltage-sensing domain relaxation would be dynamically modulated during exposure to SOL.

According to previous pharmacokinetic studies, the peak plasma concentrations of SOL with 24.0 ng/mL (0.066 µM) or 40.6 ng/mL (0.11 µM) were reported to reach 3–8 h after long-term oral administration of a 5 or 10 mg SOL dose, respectively [7,74–76]. The SOL plasma level was also found to be even higher (i.e., around 52 ng/mL or 0.14 µM) in patients with renal insufficiency [77]; and, it could have a long duration of action as it is usually taken once daily. As such, it is possible that, apart from interfering with the binding to muscarinic receptors, SOL-mediated stimulation of $I_{K(M)}$ is of clinical or therapeutic relevance.

Considering all of the experimental results together, the effects of SOL on $I_{K(M)}$ demonstrated herein appears to be acute and robust in onset; moreover, meanwhile, such stimulatory actions tend to be non-canonical and they are presumably mediated via a mechanism

independent of its blockade of muscarinic receptors. These actions probably result in its perturbations on the functional activities of electrically excitable cells (e.g., GH_3 or mHippoE-14 cells), in the case that in vivo findings occur. Whether the impairment of cognitive function after long-term administration of SOL [20–31] could be intimately connected with its stimulation of $I_{K(M)}$ in central neurons remains to be further investigated.

It is worth noting that different types of smooth muscle cells, including smooth myocytes of the urinary bladder, have been demonstrated to be functionally expressed in the activity of K_M (KCNQx) channels [52,53,78–89]. The SOL-induced interaction with K_M channels to modify the magnitude and gating of $I_{K(M)}$ has the propensity to change muscarinic cholinergic activation involved in the micturition reflex, presuming that the in vivo results happen. It turns out that whether the actions of SOL or other structurally similar compounds (e.g., darifenacin) on overactive bladder or neurogenic detrusor overactivity [90] are related to its enhanced actions on K_M-channel activity [82–85], warrants further investigations, despite its high-affinity binding to muscarinic receptors.

4. Materials and Methods

4.1. Chemicals, Drugs and Solutions Used in This Work

Solifenacin (Vesicare®, UNII-A8910SQJ1U, YM-905, [(3R)-1-azabicyclo[2.2.2]octan-3-yl] (1S)-1-phenyl-3,4-dihydro-1H-isoquinoline-2-carboxylate, 2(1H)-isoquinolinecarboxylic acid, 3,4-dihydro-1-phenyl-,1-azabicyclo(2.2.2.)oct-3-yl ester, (R-(R*,S*))-905, quinculidin-3′-yl-1-phenyl-1,2,3,4-tetrahydroisoquinoline-2-carboxylate, $C_{23}H_{26}N_2O_2$, CAS No. 242478-37-1, Solifenacin. Available online: https://pubchem.ncbi.nlm.nih.gov/compound/Solifenacin (accessed on 14 November 2021)) was supplied by MedChemExpress (Asia Bioscience, Taipei, Taiwan), the chemical structure of which is illustrated in Figure 1. Linopirdine (Lino), tetrodotoxin (TTX), thyrotropin releasing hormone (TRH) and tolbutamide (TLB) were acquired from Sigma-Aldrich (Merck, Taipei, Taiwan), and iberiotoxin (Iber) and apamin (Apa) were from Alomone (Asia Bioscience, Taipei, Taiwan). Naringenin (NGEN) was acquired from MP Biomedicals (Cold Spring, New Taipei City, Taiwan), while ML213 (N-(2,4,6-trimethylphenyl)-bicyclo[2.2.1]hepane-2-carboxamide) was from Tocris (Union Biomed, Taipei, Taiwan). Chlorotoxin (ChTx) was kindly provided by Professor Dr. Woei-Jer Chuang (Department of Biochemistry, National Cheng Kung University Medical College, Tainan, Taiwan). Unless stated otherwise, culture media (e.g., Ham's F-12 or Dulbecco's modified Eagle's medium), fetal bovine calf serum, horse serum, L-glutamine, and trypsin/EDTA were supplied by HyClone™ (Thermo Fisher; Level Biotech, Tainan, Taiwan), whereas other chemicals such as $CdCl_2$, aspartic acid, and HEPES, were of the best available quality, mostly at analytical grade.

The ion composition of extracellular solution (i.e., HEPES-buffered normal Tyrode's solution) was as follows (in mM): NaCl 136.5, $CaCl_2$ 1.8, KCl 5.4, $MgCl_2$ 0.53, glucose 5.5, and HEPES-NaOH buffer 5 (pH 7.4). To record the flowing through $I_{K(M)}$, the patch electrodes were backfilled with the following intracellular solution (in mM): K-aspartate 130, KCl 20, $MgCl_2$ 1, KH_2PO_4 1, Na_2ATP_3, Na_2GTP 0.1, EGTA 0.1, and HEPES-KOH buffer 5 (pH 7.2). To measure $I_{K(M)}$, we used a high K^+-bathing solution containing the following (in mM): KCl 145, $MgCl_2$ 0.53, and HEPES-KOH buffer 5 (pH 7.4). To record the activity of single K_M channels, the pipette solution was composed of the following (in mM): NaCl 136.5, KCl 5.4, $MgCl_2$ 0.53, and HEPES-NaOH buffer 5 (pH 7.4). All solutions used in this work were prepared in deionized water from a Milli-Q® water purification system (Merck Millipore, Taipei, Taiwan). The pipette solution and culture media were always filtered with Acrodisc® syringe filter which contains 0.2-μm Supor® nylon membrane (#4612; Pall Corporation; Genechain Biotechnology, Kaohsiung, Taiwan).

4.2. Cell Preparations

The GH_3 pituitary cell line was supplied by the Bioresources Collection and Research Center (BCRC-60015; Hsinchu, Taiwan), while the embryonic mouse hippocampal cell line (mHippoE-14, CLU198) was from Codarlane CELLutions Biosystems, Inc. (Burlington,

ON, Canada) [71]. GH$_3$ cell line was originally derived from the American Type Culture Collection (ATCC$^®$ [CCL-82.1TM]; Manassas, VA, USA). GH$_3$ cells were cultured in Ham's F-12 medium supplemented with 2.5% fetal calf serum (*v/v* percent), 15% horse serum (*v/v* percent), and 2 mM L-glutamine, while mHippoE-14 neurons were in Dulbecco's modified Eagle's medium supplemented with 10% fetal bovine serum (*v/v* percent) and 2 mM L-glutamine. Cells were grown at 37 $^\circ$C in a humidified environment of 5% CO$_2$/95% air.

4.3. Electrophysiological Measurements

GH$_3$ cells or mHippoE-14 neurons were gingerly harvested and cell suspension was rapidly placed in a customized chamber immediately before the electrical recordings. The recording chamber was positioned on the stage of an inverted DM-IL fluorescence microscope (Leica, Uranus Technology, Taipei, Taiwan) coupled to a digital video system (DCR-TR30; Sony, Tokyo, Japan) with a magnification of up to 1500×. Cells were kept immersed at room temperature (20–25 $^\circ$C) in normal Tyrode's solutions containing 1.8 mM CaCl$_2$, and the composition of this solution is stated above. The patch-clamp procedure in either whole-cell (voltage- and current-clamp mode) or cell-attached configuration was implemented by using an RK-400 patch amplifier (Biologic, Echirolles, France) [51,91]. When filled with internal solution, patch-clamp glass pipettes had tip resistances ranging between 3 and 5 MΩ and they were made from Kimax-51 capillaries (#34500 [1.5–1.8 mm in outer diameter]; Dogger, Tainan, Taiwan), by using either a PP-830 vertical puller (Narishige, Tokyo, Japan) or a P-97 horizontal puller (Sutter, Novato, CA, USA), and their tips were fire-polished with an MF-83 microforge (Narishige). The potentials were corrected for the liquid–liquid junction potential which emerged when the composition of the pipette solution was different from that in the bath. An anti-vibration air table was used to ensure mechanical stability during the measurements.

4.4. Data Recordings

The signals comprising voltage and current tracings were monitored on an HM-507 oscilloscope (Hameg, East Meadow, NY, USA) and stored online in an ASUS ExpertBook laptop computer (P2451F; ASUS, Tainan, Taiwan) at 10 kHz interfaced with a Digidata 1440A converter (Molecular Devices; Bestogen Biotech, New Taipei City, Taiwan), which proceeded for efficient analog-to-digital/digital-to-analog (AD/DA) conversion. During the measurements, the process in data acquisition equipped with this device was controlled by pCLAMP 10.6 program suite (Molecular Devices) run under Windows 7 (Redmond, WA, USA), and the signals were simultaneously displayed on an LCD monitor through USB type-C connection. Current signals were low-pass filtered at 2 kHz with an FL-4 four-pole Bessel Filter (Dagan, Minneapolis, MN, USA) to minimize possible electrical interference. After the recorded data were digitally collected, we off-line collated them using various analytical tools that include LabChart 7.0 program (ADInstruments; KYS Technology, Taipei, Taiwan), OriginPro$^®$ 2021 (OriginLab; Scientific Formosa, Kaohsiung, Taiwan) and varying custom-made macros built in Excel$^®$ 2021 under Microsoft 365 (Redmond, WA, USA).

4.5. Whole-Cell Current Analyses

To evaluate the effect of concentration-dependent stimulation of SOL on I$_{K(M)}$, GH$_3$ cells were allowed to be immersed in high-K$^+$ (145 mM K$^+$), Ca^{2+}-free solution. As the whole-cell mode was established, each cell was voltage-clamped at a holding potential of −50 mV, and a 1-sec depolarizing voltage command to −10 mV was delivered to it. The amplitude of I$_{K(M)}$ at the end-pulse of 1-sec depolarizing pulse measured during cell exposure to 10 μM SOL was taken as 100%, and current amplitudes were thereafter

compared to those in the presence of different SOL concentrations. The concentration required to increase the $I_{K(M)}$ amplitude by 50% was determined by use of the Hill function:

$$Percentage\ increase\ (\%) = \frac{E_{max} \times [SOL]^{n_H}}{EC_{50}^{n_H} + [SOL]^{n_H}}$$

where [*SOL*] is the *SOL* concentration applied, E_{max} the maximal increase in $I_{K(M)}$ caused by *SOL*, EC_{50} the concentration required for 50% stimulation, and n_H the Hill coefficient.

The time-dependent rate constant of forward (k_{+1}^*) or backward (k_{-1}) was broadly evaluated from the activation time constant (τ_{act}) of $I_{K(M)}$ activated by the long depolarizing pulse from −50 to −10 mV. The τ_{act} values in the presence of different SOL concentrations were approximated by fitting single exponential function to the trajectory of each current trace. Since a Hill coefficient of about 1 was found according to the concentration-dependent curve, the forward or backward rate constant was extended to be determined using the following equation:

$$\frac{1}{\tau_{act}} = k_{-1} + k_{+1}^* [SOL]$$

where [*SOL*] is the *SOL* concentration applied, and k_{+1}^* or k_{-1} was gained from the slope and the *y*-axis intercept at [*SOL*] = 0 of the interpolated regression line, where the relation of the reciprocal time constant of $I_{K(M)}$ activation (1.e., $1/\tau_{act}$) versus different *SOL* concentration was constructed.

The relationship of the membrane potential versus the $I_{K(M)}$ conductance gained in the absence or presence of *SOL* was well approximated by a modified Boltzmann function (or the Fermi-Dirac distribution) of the following form:

$$\frac{G}{G_{max}} = \frac{1}{1 + exp\left[\frac{-(V-V_{1/2})qF}{RT}\right]}$$

where *G* is the $I_{K(M)}$ conductance, G_{max} the maximal conductance of $I_{K(M)}$, $V_{1/2}$ the voltage at which half-maximal activation of the current is achieved, *q* the apparent gating charge, *F* Faraday's constant, *R* the universal gas constant, and *T* the absolute temperature.

4.6. Analyses of Single M-Type K+ (KM) Channels

Single K_M-channel currents experimentally measured from GH_3 cells were collated using pCLAMP 10.7 suite (Clampfit 10.7 subroutine). We determined single-channel amplitude taken with or without the addition of SOL by reliably fitting Gaussian distributions to the amplitude histograms of the closed (resting) or open state. The channel open probabilities were defined as N·PO, which was determined by using the following expression:

$$N \cdot P_O = \frac{A_1 + 2A_2 + 3A_3 + \ldots + nA_n}{A_0 + A_1 + A_2 + \ldots A_n}$$

where N is a number of active K_M channels residing in the patch examined, A_0 is an area under the curve of an all-points histogram corresponding to the closed (resting) state, and $A_1 \ldots A_n$ represents a histogram area that corresponds to the level of distinct open state for 1 to n channels in the patch. The single-channel conductance of K_M channels with or without the *SOL* addition was calculated using a linear *I-V* approximation with mean values of single-channel amplitudes measured at the different membrane potentials relative to the bath, while open lifetime distribution of K_M channels was fitted with single exponential function.

4.7. Curve-Fitting Procedures and Statistical Analyses

Linear (e.g., single-channel conductance) or nonlinear (e.g., Hill or Boltzmann equation and single exponential) curves fitting to experimental data sets demonstrated here was performed from the goodness-of-fit test using either the Solver add-in bundled with

Excel® 2021 (Microsoft) or OriginPro® 2021 (OriginLab). The values are provided as means ± standard error of mean (SEM) with sample sizes (*n*), which represents the cell number collected. The Student's t-test (paired or unpaired) or analysis of variance (ANOVA-1 or ANOVA-2) followed by post-hoc Fisher's least-significance difference test for multiple-range comparisons, was implemented for the statistical evaluation. Statistical analyses were performed using IBM SPSS version 20.0 (IBM Corp., Armonk, NY, USA). Probability with $p < 0.05$ was considered statistically significant, unless noted otherwise.

Author Contributions: Conceptualization, S.-N.W., H.-Y.C. and T.-H.C.; methodology, S.-N.W.; software, S.-N.W.; validation, H.-Y.C., T.-H.C. and S.-N.W.; formal analysis, S.-N.W.; investigation, H.-Y.C., T.-H.C. and S.-N.W.; resources, S.-N.W.; data curation, S.-N.W.; writing—original draft preparation, S.-N.W.; writing—review and editing, H.-Y.C., T.-H.C. and S.-N.W.; visualization, H.-Y.C., T.-H.C. and S.-N.W.; supervision, S.-N.W.; project administration, S.-N.W.; funding acquisition, S.-N.W. All authors have read and agreed to the published version of the manuscript.

Institutional Review Board Statement: Not applicable.

Informed Consent Statement: Not applicable.

Data Availability Statement: Not applicable.

Conflicts of Interest: The authors declare no conflict of interest.

Abbreviations

ACh	acetylcholine
ANOVA	analysis of variance
AP	action potential
Apa	apamin
ChTx	chlorotoxin
EC_{50}	the concentration required for 50% stimulation
I-V	current versus voltage
Iber	iberiotoxin
$I_{K(M)}$	M-type K^+ current
K_D	dissociation constant
K_M channel	M-type K^+ channel
Lino	linopirdine
SEM	standard error of mean
SOL	solifenacin (Vesicare®)
TLB	tolbutamide
TRH	thyrotropin releasing hormone
τ_{act}	activation time constant
TTX	tetrodotoxin
V_{hys}	voltage-dependent hysteresis

References

1. Chilman-Blair, K.; Bosch, J.L.H.R. Solifenacin: Treatment of overactive bladder. *Drugs Today* **2004**, *40*, 343. [CrossRef]
2. Simpson, D.; Wagstaff, A.J. Solifenacin in Overactive Bladder Syndrome. *Drugs Aging* **2005**, *22*, 1061–1069. [CrossRef]
3. Kreder, K.J. Solifenacin. *Urol. Clin. N. Am.* **2006**, *33*, 483–490. [CrossRef]
4. Payne, C.K. Solifenacin in Overactive Bladder Syndrome. *Drugs* **2006**, *66*, 175–190. [CrossRef]
5. Kennelly, M.J.; DeVoe, W.B. Overactive Bladder: Pharmacologic Treatments in the Neurogenic Population. *Rev. Urol.* **2008**, *10*, 182–191.

6. Pelman, R.S.; Capo, J.P., Jr.; Forero-Schwanhaeuser, S. Solifenacin at 3 years: A review of efficacy and safety. *Postgrad. Med.* **2008**, *120*, 85–91. [CrossRef]

7. Doroshyenko, O.; Fuhr, U. Clinical Pharmacokinetics and Pharmacodynamics of Solifenacin. *Clin. Pharmacokinet.* **2009**, *48*, 281–302. [CrossRef]

8. Morales-Olivas, F.J.; Estañ, L. Solifenacin pharmacology. *Arch. Esp. Urol.* **2010**, *63*, 43–52. [CrossRef]

9. Abrams, P.; Andersson, K.-E. Muscarinic receptor antagonists for overactive bladder. *BJU Int.* **2007**, *100*, 987–1006. [CrossRef]

10. Luo, D.; Liu, L.; Han, P.; Wei, Q.; Shen, H. Solifenacin for overactive bladder: A systematic review and meta-analysis. *Int. Urogynecol. J.* **2012**, *23*, 983–991. [CrossRef]

11. Abrams, P.; Kelleher, C.; Staskin, D.; Rechberger, T.; Kay, R.; Martina, R.; Newgreen, D.; Paireddy, A.; van Maanen, R.; Ridder, A. Combination Treatment with Mirabegron and Solifenacin in Patients with Overactive Bladder: Efficacy and Safety Results from a Randomised, Double-blind, Dose-ranging, Phase 2 Study (Symphony). *Eur. Urol.* **2015**, *67*, 577–588. [CrossRef]

12. Drake, M.J.; Chapple, C.; Esen, A.A.; Athanasiou, S.; Cambronero, J.; Mitcheson, D.; Herschorn, S.; Saleem, T.; Huang, M.; Siddiqui, E.; et al. Efficacy and Safety of Mirabegron Add-on Therapy to Solifenacin in Incontinent Overactive Bladder Patients with an Inadequate Response to Initial 4-Week Solifenacin Monotherapy: A Randomised Double-blind Multicentre Phase 3B Study (BESIDE). *Eur. Urol.* **2016**, *70*, 136–145. [CrossRef]

13. Herschorn, S.; Chapple, C.R.; Abrams, P.; Arlandis, S.; Mitcheson, D.; Lee, K.-S.; Ridder, A.; Stoelzel, M.; Paireddy, A.; Van Maanen, R.; et al. Efficacy and safety of combinations of mirabegron and solifenacin compared with monotherapy and placebo in patients with overactive bladder (SYNERGY study). *BJU Int.* **2017**, *120*, 562–575. [CrossRef]

14. Gratzke, C.; van Maanen, R.; Chapple, C.; Abrams, P.; Herschorn, S.; Robinson, D.; Ridder, A.; Stoelzel, M.; Paireddy, A.; Yoon, S.J.; et al. Long-term Safety and Efficacy of Mirabegron and Solifenacin in Combination Compared with Monotherapy in Patients with Overactive Bladder: A Randomised, Multicentre Phase 3 Study (SYNERGY II). *Eur. Urol.* **2018**, *74*, 501–509. [CrossRef]

15. Yamada, S.; Ito, Y.; Nishijima, S.; Kadekawa, K.; Sugaya, K. Basic and clinical aspects of antimuscarinic agents used to treat overactive bladder. *Pharmacol. Ther.* **2018**, *189*, 130–148. [CrossRef]

16. Wang, J.; Zhou, Z.; Cui, Y.; Li, Y.; Yuan, H.; Gao, Z.; Zhu, Z.; Wu, J. Meta-analysis of the efficacy and safety of mirabegron and solifenacin monotherapy for overactive bladder. *Neurourol. Urodyn.* **2019**, *38*, 22–30. [CrossRef]

17. Aschenbrenner, D.S. New Indication for Solifenacin. *AJN Am. J. Nurs.* **2020**, *120*, 24–25. [CrossRef]

18. Mirzaei, M.; Daneshpajooh, A.; Anvari, S.O.; Dozchizadeh, S.; Teimorian, M. Evaluation of the Clinical Efficacy and Complications of Duloxetine in Comparison to Solifenacin in the Treatment of Overactive Bladder Disease in Women: A Randomized Clinical Trial. *Urol. J.* **2021**, 6274. [CrossRef]

19. Zhang, Y.; Wang, S.; Zu, S.; Zhang, C. Transcutaneous electrical nerve stimulation and solifenacin succinate versus solifenacin succinate alone for treatment of overactive bladder syndrome: A double-blind randomized controlled study. *PLoS ONE* **2021**, *16*, e0253040. [CrossRef]

20. Pagoria, D.; O'Connor, R.C.; Guralnick, M.L. Antimuscarinic Drugs: Review of the Cognitive Impact When Used to Treat Overactive Bladder in Elderly Patients. *Curr. Urol. Rep.* **2011**, *12*, 351–357. [CrossRef]

21. Park, J.-W. The Effect of Solifenacin on Cognitive Function following Stroke. *Dement. Geriatr. Cogn. Disord. Extra* **2013**, *3*, 143–147. [CrossRef]

22. Kachru, N.; Carnahan, R.; Johnson, M.L.; Aparasu, R.R. Potentially inappropriate anticholinergic medication use in older adults with dementia. *J. Am. Pharm. Assoc.* **2015**, *55*, 603–612. [CrossRef]

23. Kachru, N.; Holmes, H.M.; Johnson, M.L.; Chen, H.; Aparasu, R.R. Risk of Mortality Associated with Non-selective Antimuscarinic medications in Older Adults with Dementia: A Retrospective Study. *J. Gen. Intern. Med.* **2020**, *35*, 2084–2093. [CrossRef]

24. Kachru, N.; Holmes, H.M.; Johnson, M.L.; Chen, H.; Aparasu, R.R. Antimuscarinic use among older adults with dementia and overactive bladder: A Medicare beneficiaries study. *Curr. Med. Res. Opin.* **2021**, *37*, 1303–1313. [CrossRef]

25. Kachru, N.; Holmes, H.M.; Johnson, M.L.; Chen, H.; Aparasu, R.R. Comparative risk of adverse outcomes associated with nonselective and selective antimuscarinic medications in older adults with dementia and overactive bladder. *Int. J. Geriatr. Psychiatry* **2021**, *36*, 684–696. [CrossRef]

26. Orme, S.; Morris, V.; Gibson, W.; Wagg, A. Managing Urinary Incontinence in Patients with Dementia: Pharmacological Treatment Options and Considerations. *Drugs Aging* **2015**, *32*, 559–567. [CrossRef]

27. Yang, Y.-W.; Liu, H.-H.; Lin, T.-H.; Chuang, H.-Y.; Hsieh, T. Association between different anticholinergic drugs and subsequent dementia risk in patients with diabetes mellitus. *PLoS ONE* **2017**, *12*, e0175335. [CrossRef]

28. Kosilov, K.; Kuzina, I.; Kuznetsov, V.; Gaynullina, Y.; Kosilova, L.; Prokofyeva, A.; Loparev, S. Cognitive functions and health-related quality of life in men with benign prostatic hyperplasia and symptoms of overactive bladder when treated with a combination of tamsulosin and solifenacin in a higher dosage. *Aging Male* **2017**, *21*, 121–129. [CrossRef]

29. Barthold, D.; Marcum, Z.A.; Gray, S.L.; Zissimopoulos, J. Alzheimer's disease and related dementias risk: Comparing users of non-selective and M3-selective bladder antimuscarinic drugs. *Pharmacoepidemiol. Drug Saf.* **2020**, *29*, 1650–1658. [CrossRef]

30. Welk, B.; McArthur, E. Increased risk of dementia among patients with overactive bladder treated with an anticholinergic medication compared to a beta-3 agonist: A population-based cohort study. *BJU Int.* **2020**, *126*, 183–190. [CrossRef] [PubMed]

31. Harnod, T.; Yang, Y.-C.; Chiu, L.-T.; Wang, J.-H.; Lin, S.-Z.; Ding, D.-C. Use of bladder antimuscarinics is associated with an increased risk of dementia: A retrospective population-based case–control study. *Sci. Rep.* **2021**, *11*, 4827. [CrossRef]

32. Soliman, M.G.; El-Abd, S.; El-Gamal, O.M.; Raheem, A.A.; Abou-Ramadan, A.R.; El-Abd, A.S. Mirabegron versus Solifenacin in Children with Overactive Bladder: Prospective Randomized Single-Blind Controlled Trial. *Urol. Int.* **2021**, *105*, 1011–1017. [CrossRef]

33. Kushmerick, C.; Romano-Silva, M.; Gomez, M.V.; Prado, M.A.M. Muscarinic regulation of Ca2+ oscillation frequency in GH3 cells. *Brain Res.* **1999**, *851*, 39–45. [CrossRef]

34. Wojcikiewicz, R.J.; Dobson, P.R.; Brown, B.L. Muscarinic acetylcholine receptor activation causes inhibition of cyclic AMP accumulation, prolactin and growth hormone secretion in GH3 rat anterior pituitary tumour cells. *Biochim. Biophys. Acta* **1984**, *805*, 25–29. [CrossRef]

35. Schlegel, W.; Wuarin, F.; Zbaren, C.; Zahnd, G.R. Lowering of Cytosolic Free Ca^{2+} by Carbachol, a Muscarinic Cholinergic Agonist, in Clonal Pituitary Cells (GH 3 Cells). *Endocrinology* **1985**, *117*, 976–981. [CrossRef] [PubMed]

36. Wolfe, S.E.; Brostrom, C.O.; Brostrom, M.A. Mechanisms of action of inhibitors of prolactin secretion in GH3 pituitary cells. I. Ca^{2+}-dependent inhibition of amino acid incorporation. *Mol. Pharmacol.* **1986**, *29*, 411–419. [PubMed]

37. Hedlund, B.; Barker, J.L. Carbachol changes spike-generation properties of GH3 pituitary cells. *Brain Res.* **1987**, *402*, 311–317. [CrossRef]

38. Hitoshi, Y.; Simmonds, S.H.; Hawthorne, J.N. The muscarinic receptor of rat pituitary GH3 cells is coupled with adenylate cyclase inhibition, but not with phosphoinositide turnover. *Biochem. Pharmacol.* **1988**, *37*, 2675–2681. [CrossRef]

39. Chou, Y.; Fong, J. Pretreatment with muscarinic receptor agonist activates a calcium-inhibitable adenylate cyclase in GH3 pituitary cells. *Biochim. Biophys. Acta* **2005**, *1722*, 148–155. [CrossRef]

40. Secondo, A.; De Mizio, M.; Zirpoli, L.; Santillo, M.; Mondola, P. The Cu–Zn superoxide dismutase (SOD1) inhibits ERK phosphorylation by muscarinic receptor modulation in rat pituitary GH3 cells. *Biochem. Biophys. Res. Commun.* **2008**, *376*, 143–147. [CrossRef] [PubMed]

41. Aragay, A.M.; Katz, A.; Simon, M.I. The G alpha q and G alpha 11 proteins couple the thyrotropin-releasing hormone receptor to phospholipase C in GH3 rat pituitary cells. *J. Biol. Chem.* **1992**, *267*, 24983–24988. [CrossRef]

42. Yatani, A.; Codina, J.; Sekura, R.D.; Birnbaumer, L.; Brown, A.M. Reconstitution of somatostatin and muscarinic receptor mediated stimulation of K+ channels by isolated GK protein in clonal rat anterior pituitary cell membranes. *Mol. Endocrinol.* **1987**, *1*, 283–289. [CrossRef] [PubMed]

43. Yatani, A.; Birnbaumer, L.; Brown, A. Direct coupling of the somatostatin receptor to potassium channels by a G protein. *Metabolism* **1990**, *39* (Suppl. 2), 91–95. [CrossRef]

44. Offermanns, S.; Gollasch, M.; Hescheler, J.; Spicher, K.; Schmidt, A.; Schultz, G.; Rosenthal, W. Inhibition of Voltage-Dependent Ca2+Currents and Activation of Pertussis Toxin-Sensitive G-Proteins via Muscarinic Receptors in GH3Cells. *Mol. Endocrinol.* **1991**, *5*, 995–1002. [CrossRef] [PubMed]

45. Wang, H.-S.; Pan, Z.; Shi, W.; Brown, B.S.; Wymore, R.S.; Cohen, I.S.; Dixon, J.E.; McKinnon, D. KCNQ2 and KCNQ3 Potassium Channel Subunits: Molecular Correlates of the M-Channel. *Science* **1998**, *282*, 1890–1893. [CrossRef]

46. Chen, H.; Smith, P.A. M-currents in frog sympathetic ganglion cells: Manipulation of membrane phosphorylation. *Br. J. Pharmacol.* **1992**, *105*, 329–334. [CrossRef] [PubMed]

47. Smith, P.A.; Chen, H.; Kurenny, D.E.; Selyanko, A.A.; Zidichouski, J.A. Regulation of the M current: Transduction mechanism and role in ganglionic transmission. *Can. J. Physiol. Pharmacol.* **1992**, *70*, S12–S18. [CrossRef]

48. Sankaranarayanan, S.; Simasko, S. Characterization of an M-like current modulated by thyrotropin- releasing hormone in normal rat lactotrophs. *J. Neurosci.* **1996**, *16*, 1668–1678. [CrossRef]

49. Selyanko, A.A.; Hadley, J.K.; Wood, I.C.; Abogadie, F.C.; Delmas, P.; Buckley, N.J.; London, B.; Brown, D.A. Two Types of K^+ Channel Subunit, Erg1 and KCNQ2/3, Contribute to the M-Like Current in a Mammalian Neuronal Cell. *J. Neurosci.* **1999**, *19*, 7742–7756. [CrossRef] [PubMed]

50. Brown, D.A.; Passmore, G.M. Neural KCNQ (Kv7) channels. *Br. J. Pharmacol.* **2009**, *156*, 1185–1195. [CrossRef]

51. Lo, Y.-C.; Lin, C.-L.; Fang, W.-Y.; Lőrinczi, B.; Szatmári, I.; Chang, W.-H.; Fülöp, F.; Wu, S.-N. Effective Activation by Kynurenic Acid and Its Aminoalkylated Derivatives on M-Type K^+ Current. *Int. J. Mol. Sci.* **2021**, *22*, 1300. [CrossRef]

52. Afeli, S.A.Y.; Malysz, J.; Petkov, G.V. Molecular Expression and Pharmacological Evidence for a Functional Role of Kv7 Channel Subtypes in Guinea Pig Urinary Bladder Smooth Muscle. *PLoS ONE* **2013**, *8*, e75875. [CrossRef]

53. Anderson, U.A.; Carson, C.; Johnston, L.; Joshi, S.; Gurney, A.M.; McCloskey, K.D. Functional expression of KCNQ (Kv7) channels in guinea pig bladder smooth muscle and their contribution to spontaneous activity. *Br. J. Pharmacol.* **2013**, *169*, 1290–1304. [CrossRef]

54. Haick, J.M.; Byron, K.L. Novel treatment strategies for smooth muscle disorders: Targeting Kv7 potassium channels. *Pharmacol. Ther.* **2016**, *165*, 14–25. [CrossRef] [PubMed]

55. Vanhoof-Villalba, S.L.; Gautier, N.M.; Mishra, V.; Glasscock, E. Pharmacogenetics of KCNQ channel activation in 2 potassium channelopathy mouse models of epilepsy. *Epilepsia* **2018**, *59*, 358–368. [CrossRef] [PubMed]

56. So, E.C.; Foo, N.P.; Ko, S.Y.; Wu, S.-H. Bisoprolol, Known to Be a Selective β_1-Receptor Antagonist, Differentially but Directly Suppresses I(K(M)) and I(K(erg)) in Pituitary Cells and Hippocampal Neurons. *Int. J. Mol. Sci.* **2019**, *20*, 657. [CrossRef]

57. Ebihara, S.; Akaike, N. Potassium currents operated by thyrotrophin-releasing hormone in dissociated CA1 pyramidal neurones of rat hippocampus. *J. Physiol.* **1993**, *472*, 689–710. [CrossRef]

58. Yu, H.; Wu, M.; Townsend, S.D.; Zou, B.; Long, S.; Daniels, J.S.; McManus, O.B.; Li, M.; Lindsley, C.W.; Hopkins, C.R. Discovery, Synthesis, and Structure–Activity Relationship of a Series of N-Aryl-bicyclo[2.2.1]heptane-2-carboxamides: Characterization of ML213 as a Novel KCNQ2 and KCNQ4 Potassium Channel Opener. *ACS Chem. Neurosci.* **2011**, *2*, 572–577. [CrossRef]

59. Hsu, H.-T.; Tseng, Y.-T.; Lo, Y.-C.; Wu, S.-N. Ability of naringenin, a bioflavonoid, to activate M-type potassium current in motor neuron-like cells and to increase BKCa-channel activity in HEK293T cells transfected with α-hSlo subunit. *BMC Neurosci.* **2014**, *15*, 135. [CrossRef]

60. Delmar, M.; Ibarra, J.; Davidenko, J.; Lorente, P.; Jalife, J. Dynamics of the background outward current of single guinea pig ventricular myocytes. Ionic mechanisms of hysteresis in cardiac cells. *Circ. Res.* **1991**, *69*, 1316–1326. [CrossRef]

61. Boucher, M.; Chassaing, C.; Chapuy, E.; Lorente, P. Effects of Quinidine, Verapamil, Nifedipine and Ouabain on Hysteresis in Atrial Refractoriness in the Conscious Dog: An Approach to Ionic Mechanisms. *Gen. Pharmacol. Vasc. Syst.* **1999**, *32*, 47–50. [CrossRef]

62. Bennekou, P.; Barksmann, T.L.; Jensen, L.R.; Kristensen, B.I.; Christophersen, P. Voltage activation and hysteresis of the non-selective voltage-dependent channel in the intact human red cell. *Bioelectrochemistry* **2004**, *62*, 181–185. [CrossRef] [PubMed]

63. Rappaport, S.M.; Teijido, O.; Hoogerheide, D.; Rostovtseva, T.K.; Berezhkovskii, A.M.; Bezrukov, S.M. Conductance hysteresis in the voltage-dependent anion channel. *Eur. Biophys. J.* **2015**, *44*, 465–472. [CrossRef]

64. Meloni, S.; Moehl, T.; Tress, W.; Franckevicius, M.; Saliba, M.; Lee, Y.H.; Gao, P.; Nazeeruddin, W.T.M.S.Y.H.L.P.G.M.K.; Zakeeruddin, S.M.; Rothlisberger, S.M.U.; et al. Ionic polarization-induced current–voltage hysteresis in CH3NH3PbX3 perovskite solar cells. *Nat. Commun.* **2016**, *7*, 10334. [CrossRef]

65. Noskov, S.Y.; Rostovtseva, T.K.; Chamberlin, A.C.; Teijido, O.; Jiang, W.; Bezrukov, S.M. Current state of theoretical and experimental studies of the voltage-dependent anion channel (VDAC). *Biochim. Biophys. Acta* **2016**, *1858 Pt B*, 1778–1790. [CrossRef]

66. Wu, S.-N.; Huang, C.-W. Editorial to the Special Issue "Electrophysiology". *Int. J. Mol. Sci.* **2021**, *22*, 2956. [CrossRef]

67. Maruyama, S.; Tsukada, H.; Nishiyama, S.; Kakiuchi, T.; Fukumoto, D.; Oku, N.; Yamada, S. In Vivo Quantitative Autora-diographic Analysis of Brain Muscarinic Receptor Occupancy by Antimuscarinic Agents for Overactive Bladder Treatment. *J. Pharmacol. Exp. Ther.* **2008**, *325*, 774–781. [CrossRef]

68. Anisuzzaman, A.S.M.; Nishimune, A.; Yoshiki, H.; Uwada, J.; Muramatsu, I. Influence of Tissue Integrity on Pharmacological Phenotypes of Muscarinic Acetylcholine Receptors in the Rat Cerebral Cortex. *J. Pharmacol. Exp. Ther.* **2011**, *339*, 186–193. [CrossRef]

69. Gingerich, S.; Kim, G.L.; Chalmers, J.A.; Koletar, M.M.; Wang, X.; Wang, Y.; Belsham, D.D. Estrogen receptor α and G-protein coupled receptor 30 mediate the neuroprotective effects of 17β-estradiol in novel murine hippocampal cell models. *Neuroscience* **2010**, *170*, 54–66. [CrossRef] [PubMed]

70. Huang, C.-W.; Lin, K.-M.; Hung, T.-Y.; Wu, S.-N. Multiple Actions of Rotenone, an Inhibitor of Mitochondrial Respiratory Chain, on Ionic Currents and Miniature End-Plate Potential in Mouse Hippocampal (mHippoE-14) Neurons. *Cell. Physiol. Biochem.* **2018**, *47*, 330–343. [CrossRef] [PubMed]

71. Lai, M.-C.; Wu, S.-N.; Huang, C.-W. The Specific Effects of OD-1, a Peptide Activator, on Voltage-Gated Sodium Current and Seizure Susceptibility. *Int. J. Mol. Sci.* **2020**, *21*, 8254. [CrossRef] [PubMed]

72. Castle, N.A. Pharmacological modulation of voltage-gated potassium channels as a therapeutic strategy. *Expert Opin. Ther. Patents* **2010**, *20*, 1471–1503. [CrossRef]

73. Chang, W.-T.; Liu, P.-Y.; Gao, Z.-H.; Lee, S.-W.; Lee, W.-K.; Wu, S.-N. Evidence for the Effectiveness of Remdesivir (GS-5734), a Nucleoside-Analog Antiviral Drug in the Inhibition of I (K(M)) or I (K(DR)) and in the Stimulation of I (MEP). *Front. Pharmacol.* **2020**, *11*, 1091. [PubMed]

74. Mistri, H.N.; Jangid, A.G.; Pudage, A.; Rathod, D.M.; Shrivastav, P.S. Highly sensitive and rapid LC–ESI-MS/MS method for the simultaneous quantification of uroselective α1-blocker, alfuzosin and an antimuscarinic agent, solifenacin in human plasma. *J. Chromatogr. B Analyt. Technol. Biomed. Life Sci.* **2008**, *876*, 236–244. [CrossRef] [PubMed]

75. Macek, J.; Ptáček, P.; Klíma, J. Determination of solifenacin in human plasma by liquid chromatography-tandem mass spectrometry. *J. Chromatogr. B Analyt. Technol. Biomed. Life Sci.* **2010**, *878*, 3327–3330. [CrossRef]

76. Tannenbaum, S.; Adel, M.D.; Krauwinkel, W.; Meijer, J.; Hollestein-Havelaar, A.; Verheggen, F.; Newgreen, D. Pharmacokinetics of solifenacin in pediatric populations with overactive bladder or neurogenic detrusor overactivity. *Pharmacol. Res. Perspect.* **2020**, *8*, e00684. [CrossRef]

77. Smulders, R.A.; Smith, N.N.; Krauwinkel, W.J.; Hoon, T.J. Pharmacokinetics, safety, and tolerability of solifenacin in patients with renal insufficiency. *J. Pharmacol. Sci.* **2007**, *103*, 67–74. [CrossRef]

78. Gopalakrishnan, M.; Shieh, C.-C. Potassium channel subtypes as molecular targets for overactive bladder and other urological disorders. *Expert Opin. Ther. Targets* **2004**, *8*, 437–458. [CrossRef]

79. Anderson, U.A.; Carson, C.; McCloskey, K.D. KCNQ Currents and Their Contribution to Resting Membrane Potential and the Excitability of Interstitial Cells of Cajal From the Guinea Pig Bladder. *J. Urol.* **2009**, *182*, 330–336. [CrossRef]

80. Rode, F.; Svalø, J.; Sheykhzade, M.; Rønn, L.C.B. Functional effects of the KCNQ modulators retigabine and XE991 in the rat urinary bladder. *Eur. J. Pharmacol.* **2010**, *638*, 121–127. [CrossRef]

81. Brickel, N.; Gandhi, P.; VanLandingham, K.; Hammond, J.; DeRossett, S. The urinary safety profile and secondary renal effects of retigabine (ezogabine): A first-in-class antiepileptic drug that targets KCNQ (K(v)7) potassium channels. *Epilepsia* **2012**, *53*, 606–612. [CrossRef]

82. Svalø, J.; Hansen, H.H.; Rønn, L.C.B.; Sheykhzade, M.; Munro, G.; Rode, F. Kv7 Positive Modulators Reduce Detrusor Overactivity and Increase Bladder Capacity in Rats. *Basic Clin. Pharmacol. Toxicol.* **2011**, *110*, 145–153. [CrossRef]

83. Svalø, J.; Bille, M.; Theepakaran, N.P.; Sheykhzade, M.; Nordling, J.; Bouchelouche, P. Bladder contractility is modulated by Kv7 channels in pig detrusor. *Eur. J. Pharmacol.* **2013**, *715*, 312–320. [CrossRef]

84. Svalø, J.; Sheykhzade, M.; Nordling, J.; Matras, C.; Bouchelouche, P. Functional and Molecular Evidence for Kv7 Channel Subtypes in Human Detrusor from Patients with and without Bladder Outflow Obstruction. *PLoS ONE* **2015**, *10*, e0117350. [CrossRef]

85. Takagi, H.; Hashitani, H. Effects of K^+ channel openers on spontaneous action potentials in detrusor smooth muscle of the guinea-pig urinary bladder. *Eur. J. Pharmacol.* **2016**, *789*, 179–186. [CrossRef]

86. Bientinesi, R.; Mancuso, C.; Martire, M.; Bassi, P.F.; Sacco, E.; Currò, D. K(V)7 channels in the human detrusor: Channel modulator effects and gene and protein expression. *Naunyn Schmiedebergs Arch. Pharmacol.* **2017**, *390*, 127–137. [CrossRef] [PubMed]

87. Provence, A.; Angoli, D.; Petkov, G.V. K(V)7 Channel Pharmacological Activation by the Novel Activator ML213: Role for Heteromeric K(V)7.4/K(V)7.5 Channels in Guinea Pig Detrusor Smooth Muscle Function. *J. Pharmacol. Exp. Ther.* **2018**, *364*, 131–144. [CrossRef]

88. Seefeld, M.A.; Lin, H.; Holenz, J.; Downie, D.; Donovan, B.; Fu, T.; Pasikanti, K.; Zhen, W.; Cato, M.; Chaudhary, K.W.; et al. Novel K(V)7 ion channel openers for the treatment of epilepsy and implications for detrusor tissue contraction. *Bioorg. Med. Chem. Lett.* **2018**, *28*, 3793–3797. [CrossRef] [PubMed]

89. Malysz, J.; Petkov, G.V. Detrusor Smooth Muscle K(V)7 Channels: Emerging New Regulators of Urinary Bladder Function. *Front. Physiol.* **2020**, *11*, 1004. [CrossRef] [PubMed]

90. Parsons, M.; Robinson, D.; Cardozo, L. Darifenacin in the treatment of overactive bladder. *Int. J. Clin. Pract.* **2005**, *59*, 831–838. [CrossRef] [PubMed]

91. Wu, S.-N.; Hsu, M.-C.; Liao, Y.-K.; Wu, F.-T.; Jong, Y.-J.; Lo, Y.-C. Evidence for Inhibitory Effects of Flupirtine, a Centrally Acting Analgesic, on Delayed Rectifier K^+ Currents in Motor Neuron-Like Cells. *Evid. Based Complement. Altern. Med.* **2012**, *2012*, 148403. [CrossRef] [PubMed]